AGU PUBLICATIONS

Water Resources Research

RESEARCH ARTICLE

10.1002/2014WR016581

Controls on the diurnal streamflow cycles in two subbasins of an alpine headwater catchment

Raphael Mutzner[1], Steven V. Weijs[1], Paolo Tarolli[2], Marc Calaf[3], Holly J. Oldroyd[1], and Marc B. Parlange[1,4]

[1]School of Architecture, Civil and Environmental Engineering, École Polytechnique Fédérale de Lausanne, Lausanne, Switzerland, [2]Department of Land, Environment, Agriculture and Forestry, University of Padova, Agripolis, Padova, Italy, [3]Department of Mechanical Engineering, University of Utah, Salt Lake City, Utah, USA, [4]Department of Civil Engineering, University of British Columbia, Vancouver, British Columbia, Canada

Key Points:
- Different diurnal streamflow cycles observed simultaneously in two subbasins
- Ice melt and evapotranspiration cycles have different characteristics
- Ice melt diurnal cycle is damped by evapotranspiration diurnal cycle

Correspondence to:
R. Mutzner,
raphael.mutzner@epfl.ch

Citation:
Mutzner, R., S. V. Weijs, P. Tarolli, M. Calaf, H. J. Oldroyd, and M. B. Parlange (2015), Controls on the diurnal streamflow cycles in two subbasins of an alpine headwater catchment, *Water Resour. Res.*, *51*, 3403–3418, doi:10.1002/2014WR016581.

Received 20 OCT 2014
Accepted 14 APR 2015
Accepted article online 16 APR 2015
Published online 8 MAY 2015

Abstract In high-altitude alpine catchments, diurnal streamflow cycles are typically dominated by snowmelt or ice melt. Evapotranspiration-induced diurnal streamflow cycles are less observed in these catchments but might happen simultaneously. During a field campaign in the summer 2012 in an alpine catchment in the Swiss Alps (Val Ferret catchment, 20.4 km^2, glaciarized area: 2%), we observed a transition in the early season from a snowmelt to an evapotranspiration-induced diurnal streamflow cycle in one of two monitored subbasins. The two different cycles were of comparable amplitudes and the transition happened within a time span of several days. In the second monitored subbasin, we observed an ice melt-dominated diurnal cycle during the entire season due to the presence of a small glacier. Comparisons between ice melt and evapotranspiration cycles showed that the two processes were happening at the same times of day but with a different sign and a different shape. The amplitude of the ice melt cycle decreased exponentially during the season and was larger than the amplitude of the evapotranspiration cycle which was relatively constant during the season. Our study suggests that an evapotranspiration-dominated diurnal streamflow cycle could damp the ice melt-dominated diurnal streamflow cycle. The two types of diurnal streamflow cycles were separated using a method based on the identification of the active riparian area and measurement of evapotranspiration.

1. Introduction

During recession events or during low flow conditions, daily or subdaily streamflow variations can take place in many different types of watersheds. The study of those variations can improve both our understanding of the processes happening at different scales and hydrological modeling [*Kirchner*, 2009]. As raised by *Lundquist and Cayan* [2002], when caused by solar radiation and temperature variations, the study of streamflow diurnal cycles can also be used to assess the impact of climate change on the watershed behavior. Streamflow or groundwater level diurnal cycles have been observed in very diverse places (see *Gribovszki et al.* [2010] for a review). For instance, *Lundquist and Cayan* [2002] detected streamflow diurnal changes in a large variety of watersheds in the Western United States featuring both snowmelt and evapotranspiration/infiltration driving processes and classified the watersheds by the diurnal cycle properties. The characteristics of the streamflow diurnal cycles can therefore serve as a comparison tool between catchments. Diurnal streamflow cycles are characterized through their amplitude, timing of the minimum or maximum streamflow [*Bren*, 1997; *Bond et al.*, 2002; *Caine*, 1992; *Graham et al.*, 2013; *Lundquist and Cayan*, 2002; *Lundquist et al.*, 2005; *Wondzell et al.*, 2007], shape and asymmetry [*Caine*, 1992; *Lundquist and Cayan*, 2002].

In alpine regions, diurnal streamflow cycles are mainly caused by ice melt or snowmelt resulting in a streamflow increase. These perturbations are observed at gauging stations with delays depending on the size of the watershed [*Lundquist et al.*, 2005]. Ice melt or snowmelt diurnal streamflow cycle characteristics have been used to study catchment-scale snowpack properties [*Caine*, 1992; *Kobayashi and Motoyama*, 1984; *Lundquist and Dettinger*, 2005], estimate hydraulic parameters of the riparian zone [*Loheide and Lundquist*, 2009], characterize the glacier drainage network [*Collins*, 1995, 1979], or to study suspended sediment transport at the snout of a glacier [*Singh et al.*, 2005]. High temporal resolution hydrological models are now able to reproduce diurnal streamflow cycles in alpine regions even though simple degree-day models remain

widely used (see *Hock* [2005] for a review). For instance, *Simoni et al*. [2011] successfully applied a modified version of the simple degree-day formulation taking into account the daily and hourly mean air temperatures to reproduce hourly ice melt and snowmelt in a high-altitude Swiss catchment. Several studies achieved more accurate results at hourly resolutions by adding a shortwave or net radiation term in the classical degree-day method [*Cazorzi and Fontana*, 1996; *Jost et al*., 2012; *Kane et al*., 1997; *Kustas et al*., 1994; *Martinec*, 1989; *Tobin et al*., 2013]. More sophisticated distributed energy balance models [*Lehning et al*., 2006; *Rigon et al*., 2006] have also successfully reproduced diurnal streamflow cycles, but are less commonly used due to the need of spatially distributed hydrometeorological forcing data. Even though the robustness of hydrological models are usually evaluated on larger time scales, diurnal streamflow cycles are of critical importance for calibration and performance evaluation of hydrological models running at hourly or higher-resolution time scales [*Reusser et al*., 2009].

Diurnal streamflow cycles characterized by a decrease in streamflow have been associated with processes such as evapotranspiration and groundwater recharge in losing streams. Diurnal streamflow cycles induced by groundwater recharge processes are related to the daily fluctuations of stream water and streambed temperatures [*Constantz et al*., 1994; *Constantz*, 1998; *Ronan et al*., 1998]. These diurnal streamflow variations are the largest when the streamflow is low and/or the hydraulic radius is small and when the stream is unshaded and highly exposed to solar radiative fluxes [*Lundquist and Cayan*, 2002].

Diurnal streamflow cycles induced by evapotranspiration have been studied for decades with diurnal groundwater level cycles in a broad range of watersheds and their origin are still investigated [*Barnard et al*., 2010; *Bren*, 1997; *Graham et al*., 2013]. Several methods have been proposed to estimate daily evapotranspiration based on diurnal groundwater level fluctuations [*White*, 1932; *Dolan et al*., 1984; *Hays*, 2003; *Gribovszki et al*., 2008; *Loheide*, 2008; *Soylu et al*., 2012; *Szilágyi et al*., 2008]. These methods can be used for the estimation of evapotranspiration at relatively low cost compared to evapotranspiration measured with fast-response sensors or lysimeters. Diurnal streamflow cycles have also been used to estimate evapotranspiration of riparian zones by simply computing the difference between the curve that connects daily maximums and actual streamflow rates [*Bond et al*., 2002; *Boronina et al*., 2005; *Cadol et al*., 2012; *Meyboom*, 1965; *Tschinkel*, 1963].

At catchment scale, evapotranspiration rates are often estimated with eddy covariance or alternatively measured with lysimeters, though both are much less common [*Brutsaert*, 1986; *Katul and Parlange*, 1992; *Parlange and Katul*, 1992; *Parlange et al*., 1995]. When measured evapotranspiration rates are available along with evaporated water estimated with the analysis of diurnal streamflow cycles, the area contributing to the overall measured evapotranspiration can be estimated [*Bond et al*., 2002; *Cadol et al*., 2012; *Stagnitti et al*., 1989; *Tsang et al*., 2014; *Weisman*, 1977]. However, few studies have tried to geographically identify those areas of active riparian evapotranspiration (see *Orellana et al*. [2012] for a review). *Tsang et al*. [2014] proposed to establish this area by applying a threshold on a modeled depth to the groundwater around the channel network, whereas *Boronina et al*. [2005] estimated this area based on land use maps. Remotely sensed infrared imagery [*Loheide and Gorelick*, 2006; *Pfister et al*., 2010] as well as field campaigns aimed at mapping the perennial portion of the stream network [*Godsey and Kirchner*, 2014; *Penna et al*., 2011] allow for better determination of the extent of the active riparian area. These riparian area estimations are critical for linking observed evapotranspiration-induced diurnal streamflow cycles to catchment-scale processes.

In general, most of the aforementioned studies have analyzed cases where only one type of diurnal streamflow cycle was observed. Hence, possible transitions from snowmelt or ice melt to evapotranspiration-dominated diurnal streamflow cycles have been poorly documented. Moreover, the two types of diurnal streamflow cycles might happen at similar times of the day, but separating them by visual inspection can be difficult, especially if one of the processes is dominant. This issue is addressed in this study by using a paired catchment approach in an intensively monitored catchment in the Swiss Alps. Previously, diurnal streamflow cycles were solely attributed to ice melt during the low flow season in this catchment [*Simoni et al*., 2011]. However, in our study, one subbasin experiences a transition from a snowmelt-dominated streamflow diurnal cycle to an evapotranspiration-dominated cycle. In the second subbasin, diurnal streamflow cycles are dominated by ice melt due to the presence of a small glacier. Based on the characteristics of the different diurnal streamflow cycles, we assess the impact of evapotranspiration on the ice melt-dominated streamflow cycle in the second subbasin.

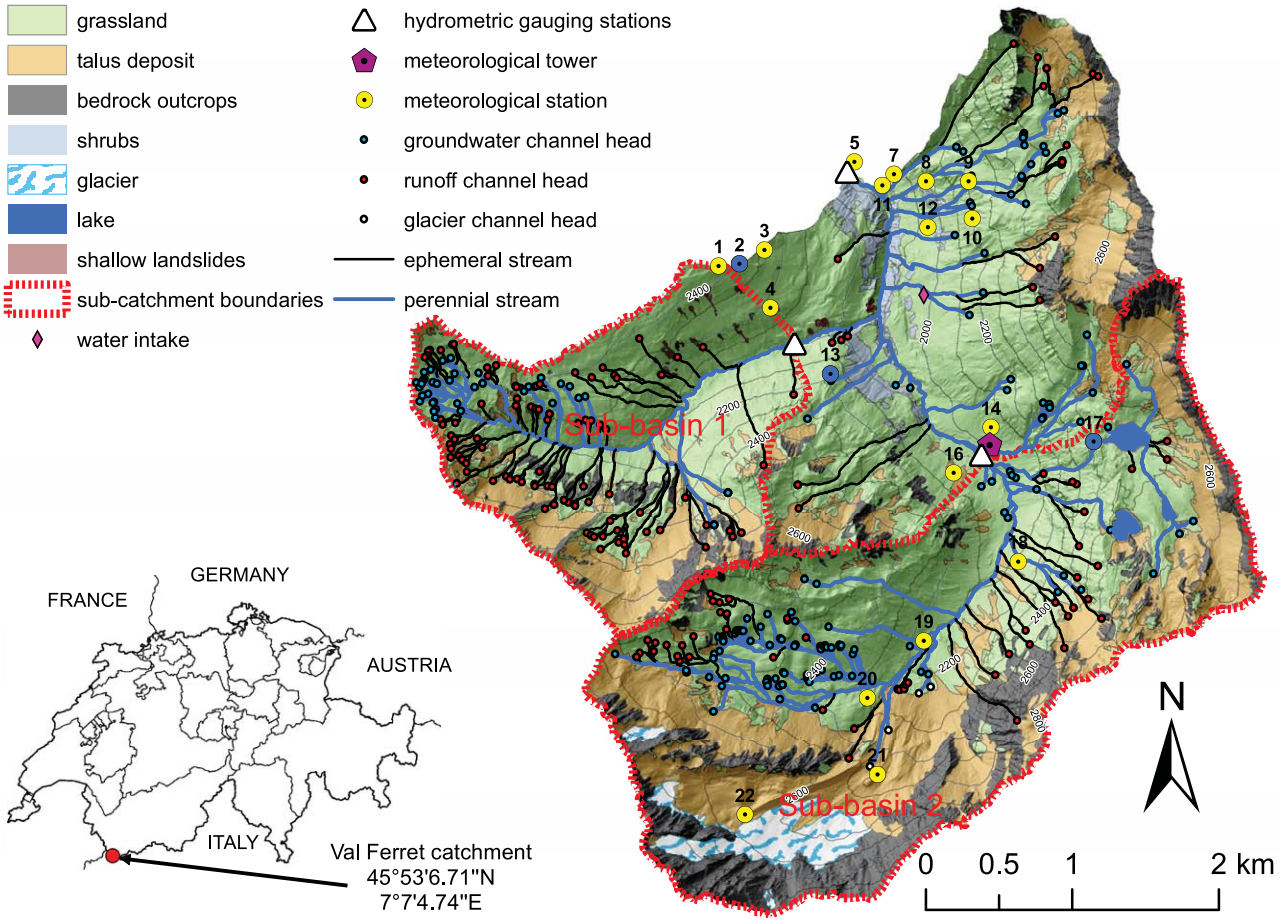

Figure 1. Map of the Val Ferret watershed showing the locations of the meteorological stations (in blue if operated during winter), the meteorological tower, the hydrometric gauging stations, the land cover, the mapped channel heads, and the channel network. The intermittent and perennial parts of the channel network are represented, respectively, by the solid black and blue lines. Based on the field observation, the channel heads have been classified as groundwater channel heads (wet, represented in blue), runoff channel heads (dry, represented in red), or glacier channel heads (wet and coming out of the moraine, represented in white).

2. Study Area and Instrumentation

2.1. The Val Ferret Watershed

Since 2009, a relatively small watershed is monitored in the Swiss Alps to study streamflow generation in steep alpine environments. The experimental site shown in Figure 1 is located in the southernmost ridge bordering Italy, covering a total surface area of 20.4 km^2 with elevations ranging from 1773 m above sea level (asl) at the outlet of the catchment to 3236 m asl at the highest point (mean elevation is 2423 m asl). The mean annual precipitation of the area is of 1360 mm. More specific details on the climatic regime of the site can be found in *Simoni et al.* [2011]. Since 2012, two subbasins of the Val Ferret catchment are also intensively monitored (see Figure 1). The land cover of the watershed is summarized in Table 1 and features a small glacier (*Glacier des Angroniettes*). The riparian area of the watershed is mainly composed of grassland, moss, and debris but almost no vegetation with deep roots. The geology of the site is complex, the strata consist mainly of sedimentary shale, quartzite, limestone, and sandstone. The analyses of several soil samples revealed a dominance of sandy silt loam and light clay types of soils. One of the appealing factors of this watershed for hydrological studies is the fact that apart from a small drinking water intake of maximum 17 L/s, there is very little anthropogenic influence on the streamflow regime.

2.2. Channel Network

The perennial channel network serves as the basis for estimating the riparian area of the subbasins (see sections 3 and 4), that is linked to an observed evapotranspiration-induced diurnal streamflow cycle. During

Table 1. Summary of Land Cover, Expressed in Percent of the Total Area, and Geomorphological Characteristics of the Watershed and the Two Monitored Subbasins[a]

	Land Cover (%)						Geomorphology		
	Grassland	Talus	Bedrock	Glacier	Lake	Shrubs	Area (km^2)	Elevation (m)	Slope (°)
Watershed	58.3	24.7	12.8	2.0	0.2	1.8	20.4	2423.2	31.6
Subbasin 1	69.7	22.9[b]	7.4	0	0	0	4.5	2357.7	31.1
Subbasin 2	43.1	32.1	19.5	4.4	0.9	0	9.3	2535.1	31.5

[a]The terms elevation and slope refer to mean values.
[b]Shallow landslides represent 0.5% of the talus deposit area of subbasin 1.

fall 2011, an intensive field observation campaign was conducted to accurately map the stream network, the location of the channel heads, and the perennial part of the stream network. The watershed was systematically walked along all the continuous drainage lines up to the catchment divide with a high-precision Global Navigation Satellite System device (based both on GPS and GLONASS with typical horizontal error of tens of centimeters) and the locations of 373 channel heads were mapped (see Figure 1). Based on the field observations, the channel heads have been classified into two main categories: (1) 183 dry runoff channel heads initiated by soil erosion or land sliding processes due to surface or subsurface runoff activated during rainfall or snowmelt events, (2) 190 wet groundwater channel heads due to groundwater surfacing process, driven by perennial flow (see Figure 2a for an illustration). Four other channel heads coming out of the moraine and fed by glacier melt were also mapped and named accordingly in Figure 1.

A 1 m resolution Lidar-derived Digital Elevation Model (DEM) and the mapped channel heads served as the basis for channel network mapping. The channel network was reconstructed by following the flow direction, i.e., the steepest path, from all channel head locations down to the outlet (see Figure 2b for an illustration). This field observation-based channel network has been used successfully in a geomorphological model predicting the properties of base flow recession events [*Mutzner et al.*, 2013]. According to the channel head type and field survey, i.e., runoff or groundwater, the channels have been classified into intermittent and perennial streams, respectively, shown in red and blue in Figure 1. Over the total network length, we observed that 52.9% of the channels are perennial, whereas the remaining 47.1% are intermittent.

2.3. Meteorological Data

The watershed has been heavily monitored since 2009 with a wireless network of small meteorological stations (Sensorscope stations [*Ingelrest et al.*, 2010]) distributed over the entire catchment (see Figure 1). In the Val Ferret catchment, these stations were previously used to study the impact of the spatial variability of air temperature and precipitation on a simple hydrological model [*Simoni et al.*, 2011] to improve snowmelt modeling based on the degree method [*Tobin et al.*, 2013] and to analyze extreme rainfall events [*Thibaud et al.*, 2013]. These stations were also used in an urban environment to study the spatial variability of sensible heat flux [*Nadeau et al.*, 2009]. The stations typically provide near-surface air temperature and

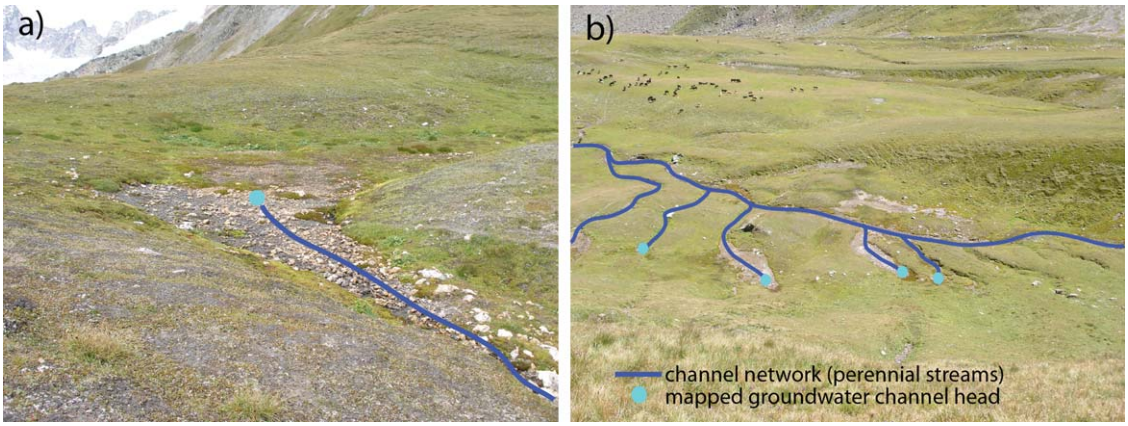

Figure 2. Examples of (a) a mapped groundwater channel head and (b) a mapped part of the watershed with a high density of groundwater surfacing channel heads and large riparian area. Both pictures were taken in the westernmost part of subbasin 2.

humidity, wind speed and direction, incoming short-wave radiation, surface temperature, rainfall, soil moisture, soil temperature, and soil water potential at a temporal resolution of 1 min. In this particular study, data of near-surface air temperature and rainfall are used, both measured at all stations. Rainfall is measured with an unheated tipping bucket rain gauge (Davis Rain Collector II) installed 0.4 m above the ground. The air temperature measurements were collected at 1.5 m above the surface using a Sensirion SHT75 sensor protected by a radiation shield.

The locations of the stations were determined to best represent catchment morphological features in terms of slope, aspect, and elevation. For most of the stations, it is not possible to maintain them during winter due their exposure to avalanche activity. Most of the stations are therefore usually deployed in late spring and uninstalled in the fall. During the 2012 campaign, all the stations were deployed after 5 June and most of them uninstalled 23 October, 18 days before uninstalling the stream water level sensors (see the following section). This was done for logistical and safety reasons to avoid the snowfalls and resulting difficult access to remote parts of the watershed and possible avalanche activity. To capture snowmelt processes, three stations were maintained during the winter, namely stations 2, 13, and 17 in Figure 1. In addition, two automatic cameras were installed at station 2, facing south-east and south-west directions, respectively. Photographs were recorded at a resolution of 10 megapixels every 2 h during daytimes of the entire period to estimate snow cover throughout the season.

During fall 2012, a short-term deployment was undertaken, aimed at isolating large coherent turbulent structures in the atmospheric boundary layer as has been previously done above a lake [*Calaf et al*., 2013]. For that purpose, a meteorological tower equipped with fast-response sensors was deployed to measure all the components of the surface energy budget and has been therefore used in this study to establish evapotranspiration rates. The station was installed at an elevation of 2004 m asl near the outlet of subbasin 2 and at 1.5 km from the outlet of subbasin 1 (see Figure 1). The station was equipped with two sonic anemometers (CSAT3,Campbell Scientific Inc, USA) mounted parallel to the surface at elevations of 2 and 4 m above ground. An open-path infrared fast-response CO_2-H_2O analyzer (Li-7500, Li-Cor, USA) was mounted with the lower sonic anemometer for eddy covariance flux measurements. The three sensors were sampling at a frequency of 20 Hz in conjunction with a CR-5000 data logger (Campbell Scientific Inc, USA) and calibrated before deployment. The station was also equipped with a four-component radiometer (Pyranometer CM21 and Pyrgeometer CG4, Kipp & Zonen B.V., The Netherlands) mounted parallel to the surface to measure the components of the radiation balance. The meteorological tower was deployed from 5 September 2012 until 6 October 2012, with a notable gap of 9 days in the data.

2.4. Streamflow Data

Stream water levels were monitored at the outlet of the catchment and at two locations upstream (see Figure 1). Water levels were recorded using pressure sensors (HyMADD, MADD Technologies, Switzerland) with a temporal resolution of one sample every 5 min. The loggers were installed inside a metal tube fixed at relatively constant cross sections of the respective catchment main rivers. The data were downloaded from the loggers and quality checked on a biweekly basis to avoid measurement errors and thermal artifacts [*Cuevas et al*., 2010; *McLaughlin and Cohen*, 2011] by comparing the logged water level with manual water level measurements. However, the water level sensor installed at the outlet of the watershed suffered from continuous fine sediment deposition during the 2012 campaign resulting in unreliable measurements, which were therefore discarded in the present study. The water level sensors of subbasin 1 and subbasin 2 were both operational from 17 July 2012 to 7 November 2012. The water level sensors were not deployed during winters because of snow and ice blockage that would lead to unreliable measurements. The water-level sensors were only operational from 17 July 2012 because of large snow accumulation in the valley floor due to avalanche activity. The streamflow was regularly measured using the salt dilution method. In total, 7 and 12 gaugings were used to model the rating curve of subbasins 1 and 2 with a power function [*Weijs et al*., 2013]. The water temperature and electrical conductivity were also monitored at the gauging stations at a temporal resolution of 5 min.

Throughout the deployment, the discharge observed at the outlet of subbasin 1 varied between 0.080 and 0.69 m^3/s (see Figure 3a). A seasonal decreasing trend in streamflow can be observed along with peaks due to rainfall events. The discharge peak of 0.69 m^3/s was measured during a rainfall event on 24 September (cumulative precipitation of 29.46 mm) accompanied by high soil moisture. At the outlet of subbasin 2, the

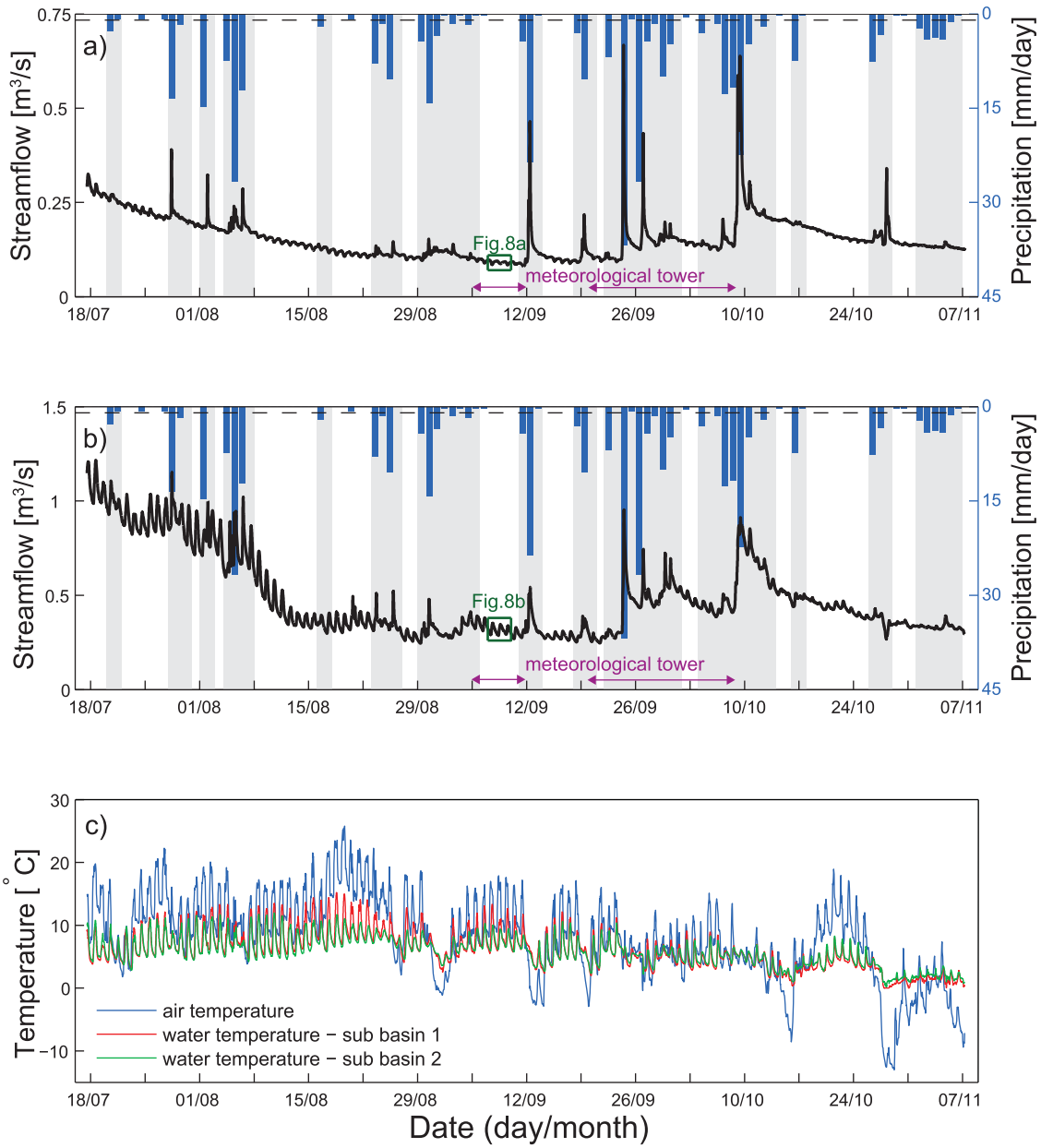

Figure 3. Time series of (a) streamflow of subbasin 1 and precipitation, (b) streamflow of subbasin 2 and precipitation, and (c) air temperature and water temperature at the outlets of subbasin 1 and subbasin 2. The days discarded from the analysis (days with precipitation exceeding the dashed line 1 mm threshold and subsequent day, see section 2) are represented as grey areas. The purple arrows in Figures 3a and 3b correspond to periods when the meteorological tower was operational. The small green box highlights the period used as illustration in Figure 8 for estimating evapotranspirated and melted volumes of water in section 4. In Figure 3c, the black dashed line corresponds to the 0° line.

discharge varied between 1.2 and 0.24 m^3/s (see Figure 3b). Similarly to previous years, when the streamflow composition was analyzed in detail [*Simoni et al.*, 2011], the runoff was dominated by snowmelt during July, whereas groundwater release and melted water from the glacier are more dominant in the rest of the season. During the entire deployment, diurnal streamflow cycles could be observed in both subbasins 1 and 2 and are analyzed in detail in section 4.

3. Methods

This study mainly focuses on the diurnal cycle signal of the streamflow. To isolate days with relatively undisturbed diurnal cycles, days with influence of precipitation on streamflow have been discarded. To that end, the precipitation collected over all stations was integrated from a resolution of 1 min to daily

values. Only three stations were maintained after 23 October, and station 13 was chosen for its relative central location in the watershed. Days with median precipitation above 1 mm were discarded from the analysis (see Figure 3). The first subsequent day was also discarded from the analysis to avoid the steep part of the recession curve. The threshold value of 1 mm and median precipitation over all stations were used to reduce sensitivity to measurement errors of the tipping bucket rain gauges.

The daily streamflow variation is obtained by subtracting a 24 h moving average window from the measured streamflow and is referred to as detrended streamflow in the following. Several characteristics are analyzed and used to compare the two types of diurnal streamflow cycles: (1) the sign of the perturbation (increase or decrease during the day), (2) the hours of occurrence of the minimum and maximum streamflow during the day, (3) the amplitude of the diurnal streamflow cycles, defined as half the difference between maximum and minimum detrended streamflow, and (4) their shape, studied through the duration of rise and decline times of the diurnal streamflow cycles, defined as the time elapsed from minimum streamflow to next maximum streamflow occurrence for the rise time and vice versa for the decline time. We also quantify the total volume of water gained or lost due to the diurnal streamflow cycles. This is done by integrating the area between the detrended streamflow and the curve connecting two subsequent maximums (if the diurnal cycle induces a streamflow decrease) or between two subsequent minimums (if the diurnal cycle induces a streamflow increase) [*Boronina et al*., 2005; *Gribovszki et al*., 2010].

The data from the fast-response sensors installed at the meteorological tower were processed to obtain daily evapotranspiration rates. They were first estimated over 30 min periods by applying the eddy covariance method. After spike removals, the classical double rotation and tilt corrections were applied to account for errors in the deployment of the sonic anemometers. Finally, density-induced fluctuations are accounted for by applying the well-known WPL correction [*Webb et al*., 1980]. Evapotranspiration rates were then integrated to daily values for the nine rainless days according to the data available at the meteorological tower (see Figure 3).

The link between evapotranspiration and diurnal streamflow cycles characterized by a decrease of streamflow is explored by computing active areas of evapotranspiration. These are obtained dividing the volume of lost water estimated from the streamflow by the daily accumulated evapotranspiration measured at the meteorological tower. These active areas of evapotranspiration are compared to the riparian area of the subbasins. Similarly to *McGlynn and Seibert* [2003] and *Penna et al*. [2011], the riparian area is obtained from the DEM by setting a slope threshold value larger than the longitudinal mean channel slope and less than the ridge slope. To estimate the riparian area of the subbasins, we make use of the channel network that was mapped carefully (see section 2.2).

4. Results

The diurnal streamflow cycles obtained for subbasin 1 and subbasin 2 by subtracting the detrended streamflow and by considering rainless days are presented in Figures 4 and 5, respectively. In subbasin 1, the diurnal streamflow patterns varied seasonally as depicted in Figure 4. Early in the season, i.e., late July, the fluctuations are characterized by an increase of streamflow during the afternoon (see red parts in Figure 4b) and a minimum streamflow in the morning. During this period, some snow patches were still visible in the pictures taken by the automatic cameras. This increase of streamflow during the day is therefore linked to snowmelt processes. Later in the season (mid-August) when there is no snow left in the subbasin, we observe a streamflow decrease during the day, with a typical minimum in the middle of the afternoon and a maximum in the early morning (see blue parts on the right side of Figure 4b). This decrease of streamflow during the day is linked to evapotranspiration forcings. Late in the season (30 October), after a small snowfall event recorded by the automatic cameras, we observed a return to a snowmelt-dominated streamflow variation cycle (see Figure 4b).

The variation of the diurnal streamflow cycles observed at subbasin 2 is depicted in Figure 5. In subbasin 2, the fluctuations are characterized by an increase of streamflow during the day (see the increase color coded in red/orange in Figure 5b) and a streamflow minimum in the morning. The diurnal streamflow cycle in subbasin 2 is mainly due to snowmelt and ice melt from the small glacier (see Figure 1). In the following, the diurnal cycles observed in the two subbasins are analyzed in detail.

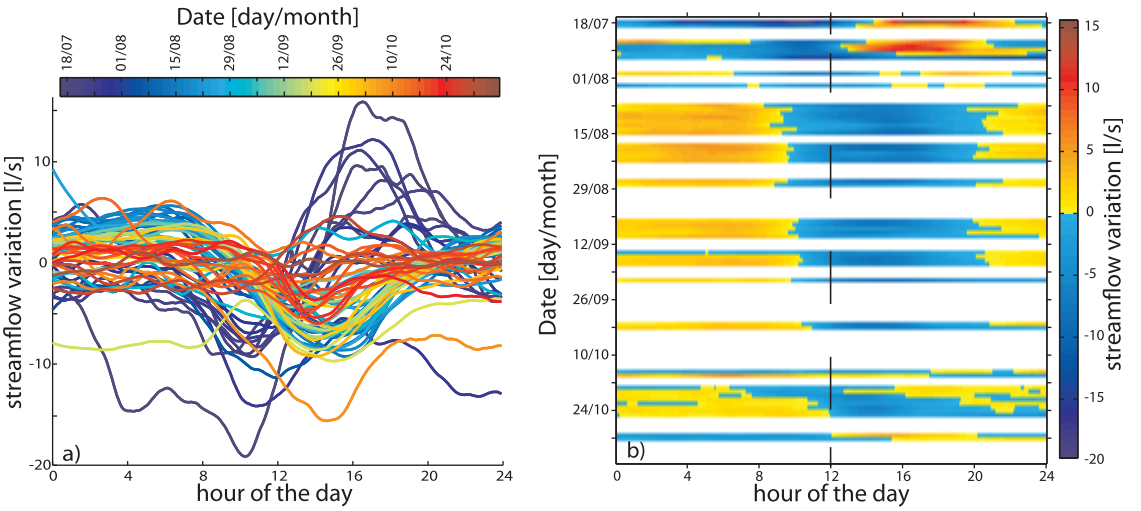

Figure 4. Observed diurnal streamflow cycles at the gauging station of subbasin 1. The streamflow variation has been obtained by subtracting a detrended streamflow hydrograph. In (a), the dates are color coded, whereas the streamflow variation is color coded in (b). The dashed line in Figure 4b corresponds to noontime.

The hour at which minimum and maximum detrended streamflow occurs is presented in Figure 6. In the case of subbasin 1 (Figure 6a), at the beginning of the season, the maximum streamflow occurs in the middle of the afternoon during the snowmelt-dominated period (median at 16 h 25 min until 29 July), whereas the minimum streamflow is observed in the morning (median at 10 h 30 min until 29 July). Afterward, three large precipitation events were observed between 29 July and 7 August (see Figure 3a). Two days with diurnal streamflow cycles were observed during this period. These two diurnal streamflow cycles were characterized by a minimum streamflow occurrence late in the morning, similar to the period dominated by snowmelt, but the maximum streamflow occurred in the early morning (see Figure 6a). After 7 August, the maximum and minimum streamflow are, respectively, observed in the early morning (median at 5 h 50 min) and in the afternoon (median at 14 h 05 min). During this period, the diurnal streamflow cycles are dominated by evapotranspiration processes. Therefore, the period between 29 July and 7 August is considered as a transition from the snowmelt-dominated period to the evapotranspiration-dominated period (see Figure 6a). During the latter period, the hour of minimum streamflow occurrence slowly shifts from the middle of the afternoon toward noon as the season progresses (-3.1 ± 1.7 min/d with uncertainty given as

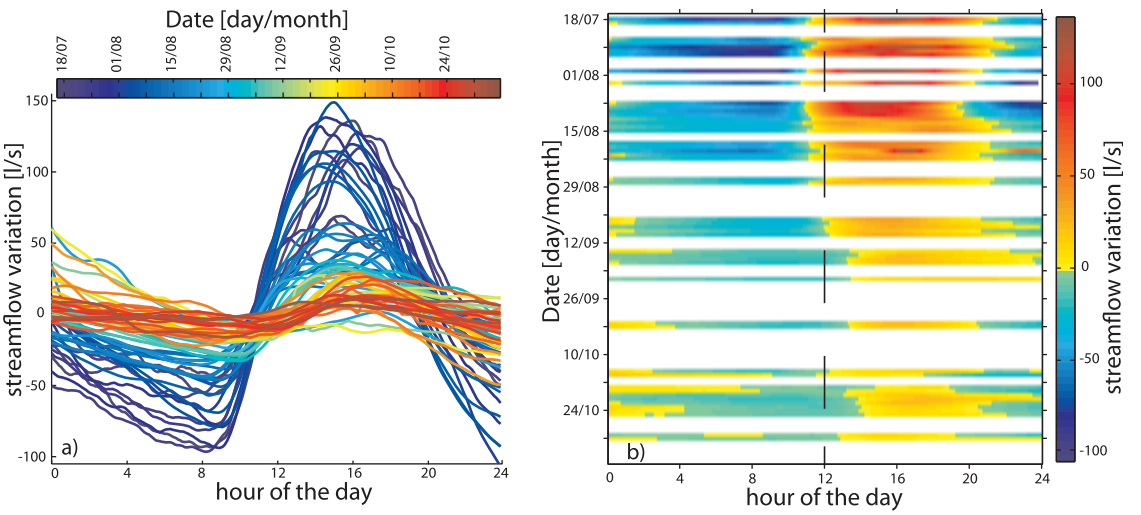

Figure 5. Observed diurnal streamflow cycles at the gauging station of subbasin 2. The streamflow variation has been obtained by subtracting a detrended streamflow hydrograph. In (a), the dates are color coded, whereas the streamflow variation is color coded in (b). The dashed line in Figure 5b corresponds to noontime.

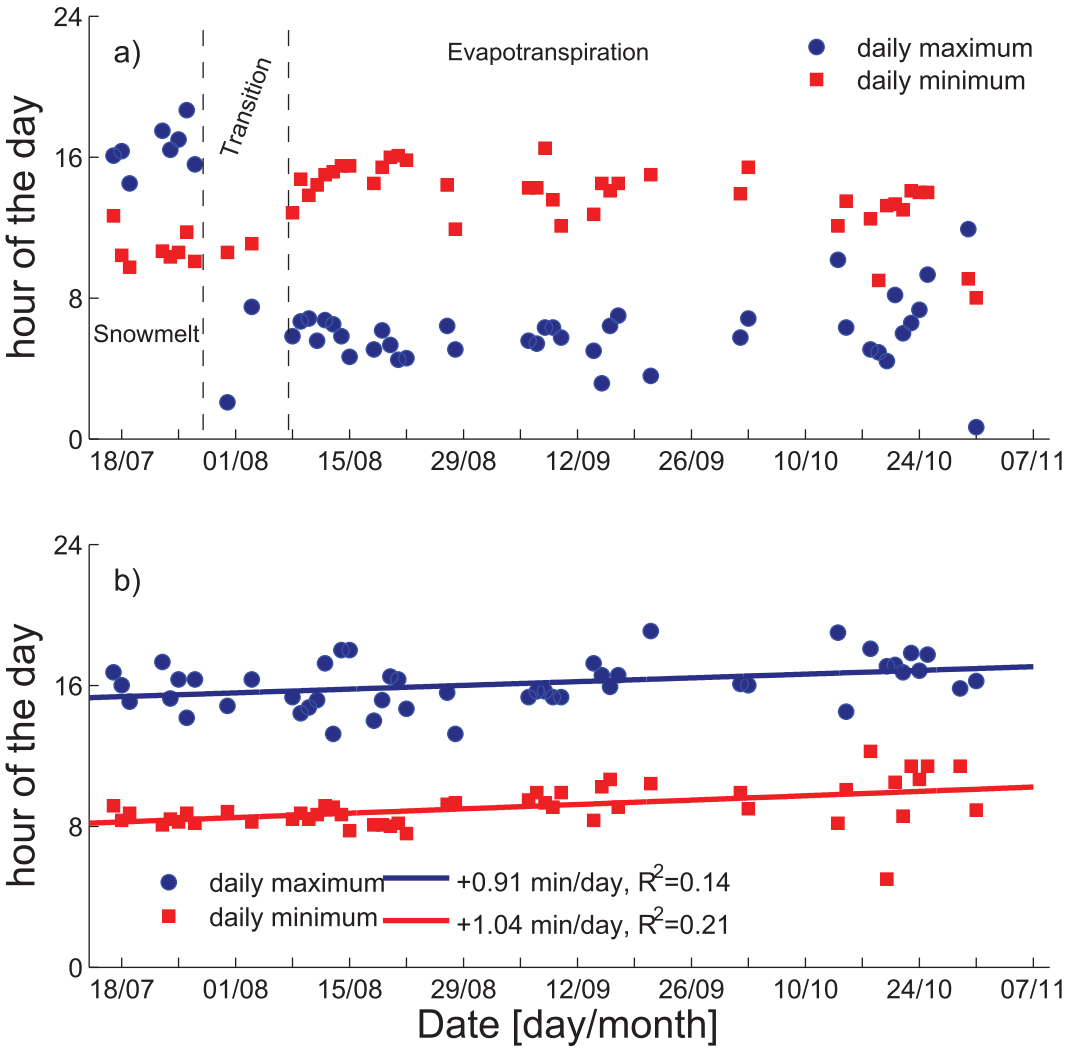

Figure 6. Hours of minimum and maximum streamflow occurrence during diurnal cycles in (a) subbasin 1, (b) subbasin 2 as a function of the time of year. The solid lines in Figure 6b represent a linear regression line. In Figure 6a, the terms *Snowmelt*, *Transition*, and *Evapotranspiration* refer to the main drivers of the streamflow diurnal cycles of subbasin 1.

95% confidence intervals here and in the following), whereas no seasonal trend was observed for the hour of maximum streamflow occurrence.

In the case of subbasin 2 (Figure 6b), the maximum and minimum streamflow occurrences are always in the afternoon and morning, respectively. The time difference between the peaks is relatively constant during the season (mean difference of 6 h 55 min, standard deviation of 1 h 40 min). However, the maximum and minimum streamflows occur later as the season progresses (daily shift of $+0.91 \pm 0.67$ min/d for the maximum and $+1.04 \pm 0.60$ min/d for the minimum). It is also noteworthy to observe from Figure 6 that the minimum streamflow of subbasin 1 tends to occur at the same time as the maximum streamflow of subbasin 2.

The amplitude of the diurnal streamflow cycles is represented in Figure 7. In the case of subbasin 1, the amplitude decreases from 16 to 5 L/s in the snowmelt-dominated period from the beginning of the season until 29 July (see Figure 7a). After 7 August, during the period dominated by evapotranspiration, the amplitude decreases slowly from values around 7 L/s toward 2–3 L/s at the end of the field campaign (with a variation of -0.037 ± 0.014 L/s/d). In the case of subbasin 2, the amplitude decreases exponentially with a decay constant of 46 ± 10 days (exponential fit with $R^2 = 0.75$, see Figure 7b). The amplitude of the diurnal signal observed in subbasin 2 was best predicted by the daily mean discharge ($R^2 = 0.53$, $p = 2.4 \times 10^{-9}$) and by the daily total incoming short-wave radiation measured at the small meteorological stations ($R^2 = 0.53$, $p = 3.2 \times 10^{-9}$) with a higher predictive power when both are combined ($R^2 = 0.79$, $p = 1.8 \times$

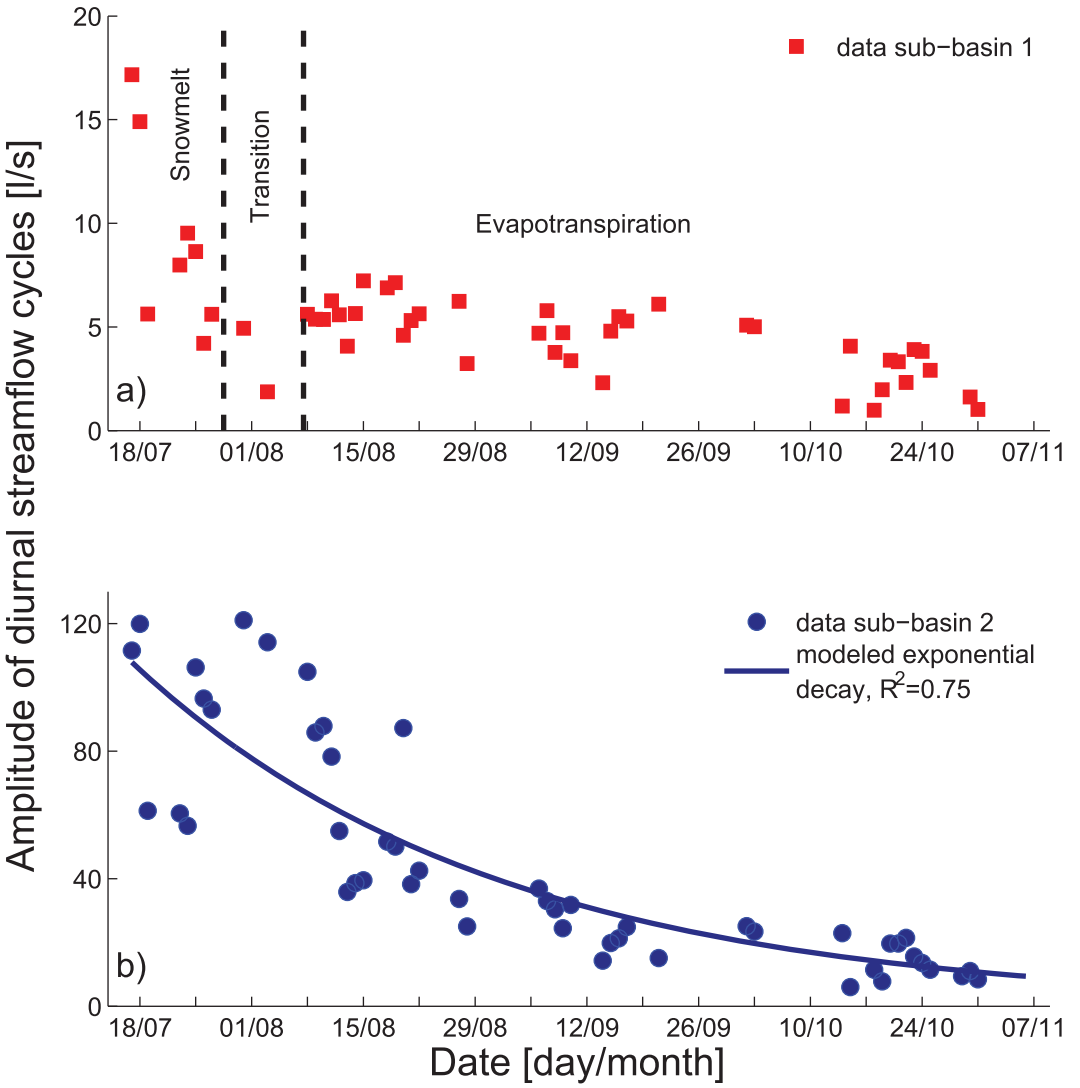

Figure 7. Amplitude of the diurnal cycle, defined as half the difference between daily maximum and minimum streamflow, as a function of the time of year for (a) subbasin 1 and (b) subbasin 2. The solid blue line in Figure 7b represents an exponential regression model. Note the difference in amplitude magnitude between the two subbasins.

10^{-15}). In contrast, the mean daily air temperature had a lower predictive power ($R^2 = 0.24$, $p = 2.9 \times 10^{-5}$), and even weaker when raised to a power of four to approximate the long-wave radiation correlation ($R^2 = 0.09$, $p = 3.4 \times 10^{-2}$).

The rise and decline times of the diurnal streamflow cycles are reported in Table 2. In the case of subbasin 1, we observe that the mean rise and decline times of the snowmelt-dominated and evapotranspiration-dominated signals are different. This illustrates that the two different cycles have a different shape, as could be observed in Figure 4a. We note that for the cases of streamflow increase during the day (i.e., the snowmelt-dominated period in subbasin 1 and the ice melt signal in subbasin 2), the diurnal streamflow cycles are characterized by a short mean rise time and a longer mean decline time. On the contrary, when the streamflow decreases during the day (i.e., the evapotranspiration-dominated period in subbasin 1), the diurnal streamflow cycles are characterized by a short mean decline time and a longer mean rise time. The two types of observed diurnal streamflow cycles are therefore characterized by faster changes in the direction of the perturbation.

In order to evaluate and decipher the origin of the evapotranspiration diurnal cycle observed in subbasin 1, volumes of evaporated water during the rainless days were estimated from the diurnal streamflow cycles as illustrated in Figure 8a. Therein, base flow is assumed to vary linearly between two consecutive maximums

Table 2. Mean Rise and Decline Times of the Diurnal Streamflow Cycles Observed in the Two Subbasins, Classified by the Dominant Process[a]

	Dominant Process	t_{rise} (h)	$t_{decline}$ (h)
Subbasin 1	Snowmelt	5.73 ± 1.93	17.52 ± 1.75
Subbasin 1	Evapotranspiration	15.98 ± 1.84	7.70 ± 2.70
Subbasin 2	Ice melt	6.99 ± 1.67	17.07 ± 1.30

[a]The uncertainty refers to the standard deviation of the rise and decline times.

of daily streamflow. These estimated volumes of water are then linked to the evapotranspiration measured through eddy covariance at the meteorological tower installed in the watershed (see Figure 1) by computing an active area of evapotranspiration. According to the data available from the meteorological tower, this active evapotranspiration area has been computed for 9 days among which five were consecutive (see Figure 3a), leading to a mean and median area of, respectively, 23.16 and 17.43 ha, corresponding, respectively, to 4.9% and 3.7% of the total subbasin area (minimum, maximum, and standard deviation of 9.31, 55.6, and 7.41 ha corresponding to 2.1% 12.1%, and 1.6% of the total subbasin area). Similar to *Tsang et al.* [2014], we make the hypothesis that this active evapotranspiration area corresponds to the riparian area of subbasin 1 and comment this assumption in section 5.

The mapped channel network is used to estimate the riparian area of subbasin 1. When considering the entire channel network length, the riverbank width should be of 5.7 m for the riparian area to be equal to the active evapotranspiration area. However, in some parts of the catchment this is not reasonable, especially in the steep intermittent streams which do not contribute to the evapotranspiration cycle since they are dry most of the time (see Figure 1). Moreover, in some areas, the riverbank width is larger, especially for the low-order channel heads (see Figure 2b for an illustration). We therefore only took into account the perennial part of the channel network which corresponds to 41% of the total network in subbasin 1. A slope threshold larger than the longitudinal mean channel slope and less than the ridge slope was set to separate the riparian and hillslope areas. By comparing results to the orthophotos and pictures taken during the channel network survey, we identified a slope threshold value of 25° to be suitable to distinguish riparian

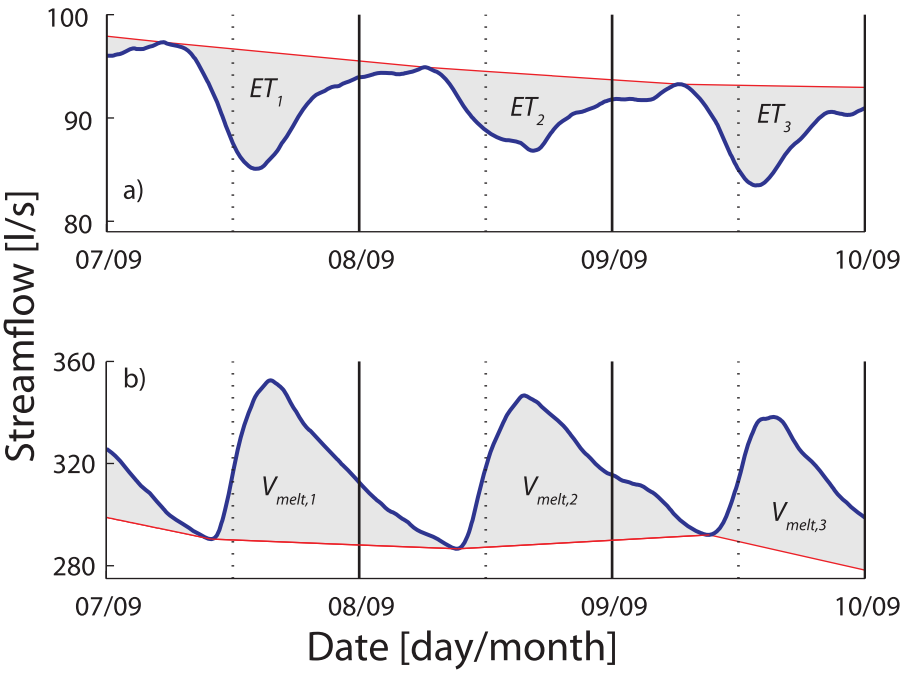

Figure 8. Examples of calculations for three consecutive days of (a) the evapotranspirated and (b) melted volumes of water. The blue and red solid lines represent the measured streamflow and the base flow, respectively. The grey area between the two lines is the volume of evapotranspirated (ET_j) in Figure 8a and melted water ($V_{melt,j}$) in Figure 8b. Vertical solid and dotted lines represent midnight and noon, respectively. Note the different axis scales between Figure 8aand Figure 8b.

and hillslope zones in the vicinity of the perennial channel network. With this threshold, we obtained a riparian area of 19.71 ha, corresponding to 4.2% of the subbasin area.

A similar procedure has been applied to subbasin 2 to study the diurnal ice melt-induced streamflow cycles. Analogous to subbasin 1, daily volumes of ice melt water were computed as illustrated in Figure 8b. Therein, base flow is assumed to vary linearly between two consecutive minimums of daily streamflow. The two subbasins represent similar geomorphology as seen in the map of Figure 1, with areas covered by rocks in the southern parts of the subbasins and grassland areas in the northern parts of the subbasins. Interestingly, there is also an area in subbasin 2 with a relatively large density of groundwater channel heads and low slopes. It is therefore possible that similar diurnal streamflow cycles occur in subbasin 2 due to evapotranspiration. However, it might not be detectable due to the larger amplitude of the ice melt diurnal streamflow cycle compared to the evapotranspiration signal of opposite sign (see Figure 7), both happening at similar times (see Figure 6). To quantify a possible underestimation of the total amount of ice melted in the glacier, we separated the observed ice melt-induced signal in a pure ice melt component and an evapotranspiration component. To estimate the latter one, we applied the same method for establishing the riparian area at the origin of the evapotranspiration diurnal streamflow cycle observed in subbasin 1. In subbasin 2, using the same slope threshold of 25° as in subbasin 1, we obtained an active evapotranspiration area of 26.9 ha, corresponding to 2.9% of the subbasin area. For the nine rainless days of reliable evapotranspiration estimated from the meteorological tower data set, an evaporated volume of water V_{ET} was computed as the product of the measured evapotranspiration rates times the active evapotranspiration area. Therefore, the total volume of ice melt water was computed as the sum of the volume of melted ice obtained from the streamflow measurements ($V_{melt,j}$ in Figure 8b) and of the evaporated volume of water V_{ET}. On average, the estimated total volume of water melted from the glacier during daytime was increased by 26%.

5. Discussion

The diurnal streamflow cycle in the Val Ferret catchment was previously attributed to ice melt during the low flow season [*Simoni et al*., 2011]. However, we observed a diurnal cycle in subbasin 1 with a decrease of streamflow during daytime mainly due to evapotranspiration. At the beginning of the season, diurnal streamflow cycles in subbasin 1 are dominated by snowmelt (see Figure 4). The amplitude of this snowmelt cycle was of the same order of magnitude as the amplitude of the evapotranspiration cycle. Unfortunately, most of the snow was already melted in subbasin 1 when the water level probes were installed so that the largest amplitudes of the snowmelt-induced diurnal streamflow cycles were not monitored. We found that the smowmelt and evapotranspiration diurnal streamflow cycles of subbasin 1 occur at different times of the day (see Figure 6a). Moreover, they are characterized by different rise and decline times (see Table 2) illustrating a different shape, in accordance with observations in Californian watersheds [*Lundquist and Cayan*, 2002]. Therefore, the evapotranspiration-dominated diurnal streamflow cycles in subbasin 1 cannot only be due to thermal artifacts as questioned by *Cuevas et al*. [2010] and *McLaughlin and Cohen* [2011]. Moreover, the transition from the snowmelt-dominated diurnal streamflow cycles to the evapotranspiration-dominated diurnal streamflow cycles happened during a short period of time characterized by similar diurnal air temperature variations. Therefore, the pressure fluctuations induced by air temperature variations resulting in erroneous waterlevel measurements should be similar for both types of diurnal cycles. A pure thermal artifact of the waterlevel decrease during the day can therefore be reasonably rejected. Furthermore, the water level probes were carefully and regularly checked to exclude seasonal drift or sediment accumulation.

Other effects such as groundwater recharge in losing reaches could also induce diurnal streamflow decrease. During the periods when streamflow decrease was observed during daytime, the measured water electrical conductivity was also decreasing in phase with the water level over a diurnal cycle. In case of groundwater recharge being the only process for streamflow decrease, the electrical conductivity should stay relatively constant during the day. Indeed, infiltration of water along all streams to the groundwater through the hyporheic zone should affect the water mass balance, but not the electrical conductivity, which reflects the water salinity. Moreover, the water temperature remained relatively cold during the campaign, fluctuating between 1.2°C and 15°C during the season with typical daily fluctuations of 7–8°C (see Figure

3c). Groundwater recharge depends on the hydraulic conductivity which is inversely proportional to the temperature-dependent water viscosity. Diurnal cycles of water temperature could therefore induce a diurnal variation of the hydraulic conductivity, resulting in diurnal patterns in groundwater recharge. However, water with low temperature has a larger water viscosity and therefore a lower hydraulic conductivity, resulting in low infiltration rates. Groundwater recharge has therefore been neglected in our study and the daily streamflow variation in sub-basin 1 has been attributed to evapotranspiration. The determination of physical mechanisms leading to such diurnal cycles are still debated and are beyond the scope of this article. The readers are referred to Graham et al. [2013] for a review of hypothetical physical mechanisms leading to evapotranspiration-induced diurnal streamflow cycles.

In subbasin 2, the diurnal streamflow cycles were mainly due to ice melt from the small glacier. During days with observed diurnal streamflow cycles, the minimum and maximum streamflow always occurred, respectively, during the morning and the afternoon (see Figure 6b), but the occurrence of minimum and maximum streamflow shifted during the season by approximately 1 min d^{-1}. This shift can be attributed to smaller water velocities as shown by the decrease of the streamflow amplitude, resulting in longer travel times, longer travel distances due to the seasonal glacier ablation, and eventually to the shift of sunrise occurrence. The amplitude of the ice melt-induced diurnal streamflow cycle in subbasin 2 decreased exponentially during the field campaign and was characterized by a large scatter (see Figure 7b). The origin of this amplitude decrease can be attributed to the seasonal glacier ablation. The seasonal decrease of the ice melt-induced diurnal cycle casts some doubts on the previous understandings of the Val Ferret catchment where the glacier contribution to total runoff was considered to be constant during the season [*Simoni et al*., 2011]. Moreover, the amplitude of the diurnal streamflow cycle was better predicted by the total incoming solar short-wave radiation than by the mean daily temperature. This supports the effort of including radiation measurements in the simple degree-day method for snowmelt or ice melt modeling.

Active areas of evapotranspiration have been computed in subbasin 1 by dividing daily volumes of evapotranspirated water by evapotranspiration measured at the meteorological station. On average, we found that this area corresponds to 4.17% of the total area of subbasin 1. While *Bond et al*. [2002] and *Boronina et al*. [2005] reported smaller values (0.1–0.7 %), our results are comparable to the values found recently by *Tsang et al*. [2014] (10% of the watershed area), but this area is very site specific, depending on the land cover and the catchment geomorphology.

Several errors can influence the estimation of the active areas of evapotranspiration. First, some errors can be introduced when computing the volumes of evapotranspirated water from the streamflow measurements. Recession flows usually exhibit an exponential streamflow decay, but the error made by discretizing the recession flow with a straight line between two subsequent days is relatively little. Moreover, this approach does not introduce any recession time scale parameter as is usually needed with the use of an exponential decay. However, this assumption results in a small overestimation of the evapotranspirated water. Finally, groundwater recharge have been ruled out as principal process for inducing the decreasing streamflow diurnal cycle, but can still contribute to streamflow losses and therefore result in a small overestimation of the evapotranspirated water. Second, some errors can be introduced by using the evapotranspiration rates measured at the meteorological station. Measurement errors of the fast-response sensors are minimized by the calibration that was done before the deployment and regular data quality checks undertaken during the deployment. The spatial variability of evapotranspiration is not considered in this study and can be of critical importance. The topographical shading and local aspect as well as land use are some factors that can vary local evapotranspiration values. However, the location of the eddy covariance tower was relatively central in the catchment. The site was comparable to both zones of subbasins 1 and 2 where a large amount of groundwater channel heads were mapped, characterized by relatively flat areas and very humid soils. The measured latent heat fluxes were generally in excess of sensible heat fluxes so that the vegetation was not moisture limited.

We attributed the evapotranspiration-induced diurnal streamflow cycles observed in subbasin 1 to the evapotranspiration in the riparian area, even though there is no physical evidence for such assumption. Several observations made evapotranspiration a plausible mechanism. During rainless periods, transpiration is high in the vegetation close to the river due to soil saturation and evaporation from streams is high in the low-order streams originating from the groundwater channel heads where the flow rate is the lowest. In particular, we observed a high density of first-order perennial streams in the westernmost part of the

subbasins as illustrated in Figure 2a. The soil around and upstream those first-order channels was always saturated and hydrologically connected to the channel network, i.e., contributing to total streamflow. Moreover, the riparian vegetation observed in subbasin 1 was characterized by relatively shallow roots (see section 2.1). A separation between the evaporation and transpiration is beyond the scope of this study but we acknowledge that the diurnal streamflow cycle might be dominated by direct evaporation from streams only, which needs further research.

To geographically identify the active evapotranspiration area, we make use of only the perennial part of the channel network which reduces the error on the riparian area estimation. Most studies rely on an objective, automatic extraction of the channel network based on a critical support area [i.e., *O'Callaghan and Mark*, 1984], which assumes constant drainage density. This classical method makes no distinction between intermittent and perennial streams, resulting in an overestimation of the riparian area, especially during low flow conditions when most of the intermittent streams are dry. Note that it is also of critical importance to use a high-resolution DEM to better recognize the channel network [*Tarolli*, 2014] and therefore reduce the error in the riparian area estimation. Moreover, we do not account for a possible temporal evolution of the riparian zone which could be induced by a temporal evolution of the channel network, especially during longer dry periods where some parts of the streams could dry out.

The comparison of the different diurnal streamflow cycles shows that the amplitude of the evapotranspiration cycle of subbasin 1 can be regarded as constant in contrast to the amplitude of the ice melt cycle of subbasin 2 (see Figure 7). However, the two types of diurnal streamflow cycles occur at similar times of the day but with an opposite sign (see Figure 6). Therefore, by visual inspection of the diurnal streamflow cycle measured at subbasin 2 alone, it is almost impossible to detect the occurrence of a diurnal streamflow cycle of evapotranspirative nature. Even though the amplitude of the evapotranspiration-induced signal was much lower than the amplitude of the ice melt-induced signal, the effect on the estimation of the daily ice melted volume of water was not negligible, with an increased volume of 26%. This was achieved by separating the observed ice melt-dominated diurnal streamflow cycle by a pure ice melt component and an evapotranspiration component. We acknowledge that this method might only be applicable in relatively small basins. In our case, the travel times are sufficiently short so that we observed occurrences of evapotranspiration and ice melt diurnal streamflow cycles at similar times of the day. In larger basins, timing and transport issues might hinder a clear separation between different types of diurnal cycles as the travel distances are longer. Indeed, for large streams and even more late in the season, snowmelt or ice melt-induced signals are subject to longer travel times and wave dispersion, resulting in a delayed appearance and perhaps less pronounced shapes of meltwater diurnal signals. In our case, the ice melt signal was induced locally by one glacier but several snowmelt or ice melt signals might be added in larger basins which could hinder the identification of diurnal streamflow cycles. Evapotranspiration signals can be induced locally, but as well by riparian areas at longer distances from the gauging station. All these factors must be considered carefully when adding and subtracting diurnal signals for establishing water mass balances, and our result suggest that evapotranspiration-induced diurnal streamflow cycles should be included when assessing conceptual models for snowmelt or ice melt.

6. Conclusions

Diurnal streamflow cycles in high alpine catchments are typically dominated by snowmelt or ice melt in the presence of glaciers. We observed a transition from a snowmelt-dominated diurnal streamflow cycle to an evapotranspiration-dominated diurnal streamflow cycle in a subbasin of a well-monitored high-altitude catchment in the Swiss Alps. The two processes induced diurnal streamflow cycles of opposite signs at similar times during the day. In another subbasin of the catchment, we observed a diurnal streamflow cycle throughout the season dominated by the ice melt from a small glacier. The amplitude of the ice melt-induced diurnal streamflow cycle was larger than the amplitude of the evapotranspiration-induced cycle. Even though the impact of the evapotranspiration cycle was not visible in the observed ice melt cycle, our study suggests that damping of the ice melt cycle by the evapotranspiration cycle is not negligible. Ice melt-dominated diurnal streamflow cycles are expected to be amplified with warming climate. It is therefore of crucial importance to obtain accurate estimates of evapotranspiration in mountainous areas for future glacier mass balance estimations and for hydrological models to correctly simulate discharge at subdaily temporal resolutions.

Acknowledgments
The authors are grateful to the Swiss National Science Foundation for financial support (grant 200021_134982/1 and 200021_153615) and to the NCCR-MICS and CCES fundings. Also, grateful acknowledgement of the NSERC discovery grant to M.B.P. The data used in this study have been entirely collected by the EFLUM laboratory of EPFL and can be obtained from Marc Parlange (marc.parlange@ubc.ca). The authors wish to thank in particular J. Golay, M. Diebold, B. Calliari, and G. Barrenetxea for their help during the field campaign. The authors wish to thank the Commune d'Orsières for providing logistic support in the Val Ferret catchment. The authors thank Jessica Lundquist, Steven Fassnacht, and two anonymous reviewers, who provided very detailed and constructive comments that improved the paper.

References

Barnard, H. R., C. B. Graham, W. J. Van Verseveld, J. R. Brooks, B. J. Bond, and J. J. McDonnell (2010), Mechanistic assessment of hillslope transpiration controls of diel subsurface flow: A steady-state irrigation approach, *Ecohydrology*, *3*(2), 133–142, doi:10.1002/eco.114.

Bond, B. J., J. A. Jones, G. Moore, N. Phillips, D. Post, and J. J. McDonnell (2002), The zone of vegetation influence on baseflow revealed by diel patterns of streamflow and vegetation water use in a headwater basin, *Hydrol. Processes*, *16*(8), 1671–1677, doi:10.1002/hyp.5022.

Boronina, A., S. Golubev, and W. Balderer (2005), Estimation of actual evapotranspiration from an alluvial aquifer of the Kouris catchment (Cyprus) using continuous streamflow records, *Hydrol. Processes*, *19*(20), 4055–4068, doi:10.1002/hyp.5871.

Bren, L. J. (1997), Effects of slope vegetation removal on the diurnal variations of a small mountain stream, *Water Resour. Res.*, *33*(2), 321–331, doi:10.1029/96WR02648.

Brutsaert, W. (1986), Catchment-scale evaporation and the atmospheric boundary layer, *Water Resour. Res.*, *22*(9S), 39S–45S, doi:10.1029/WR022i09Sp0039S.

Cadol, D., S. Kampf, and E. Wohl (2012), Effects of evapotranspiration on baseflow in a tropical headwater catchment, *J. Hydrol.*, *462–463*, 4–14, doi:10.1016/j.jhydrol.2012.04.060.

Caine, N. (1992), Modulation of the diurnal streamflow response by the seasonal snowcover of an alpine basin, *J. Hydrol.*, *137*(1–4), 245–260, doi:10.1016/0022–1694(92)90059-5.

Calaf, M., M. Hultmark, H. J. Oldroyd, V. Simeonov, and M. B. Parlange (2013), Coherent structures and the k^{-1} spectral behaviour, *Phys. Fluids*, *25*(12), 125107, doi:10.1063/1.4834436.

Cazorzi, F., and G. D. Fontana (1996), Snowmelt modelling by combining air temperature and a distributed radiation index, *J. Hydrol.*, *181*(1–4), 169–187, doi:10.1016/0022–1694(95)02913-3.

Collins, D. N. (1979), Quantitative determination of the subglacial hydrology of two alpine glaciers, *J. Glaciol.*, *23*, 347–361.

Collins, D. N. (1995), Daily patterns of discharge, solute content and solute flux in meltwaters draining from two alpine glaciers, in *Biogeochemistry of Seasonally Snow-Covered Catchments (Proceedings of a Boulder Symposium)*, IAHS publication nr 228, edited by K. A. Tonnessen, M. W. Williams, M. Tranter, vol. 228, pp. 371–378, Boulder, Colo.

Constantz, J. (1998), Interaction between stream temperature, streamflow, and groundwater exchanges in alpine streams, *Water Resour. Res.*, *34*(7), 1609–1615, doi:10.1029/98WR00998.

Constantz, J., C. L. Thomas, and G. Zellweger (1994), Influence of diurnal variations in stream temperature on streamflow loss and groundwater recharge, *Water Resour. Res.*, *30*(12), 3253–3264, doi:10.1029/94WR01968.

Cuevas, J., M. Calvo, C. Little, M. Pino, and P. Dassori (2010), Are diurnal fluctuations in streamflow real?, *J. Hydrol. Hydromech.*, *58*(3), 149–162, doi:10.2478/v10098-010-0014-0.

Dolan, T. J., A. J. Hermann, S. E. Bayley, and J. Zoltek Jr. (1984), Evapotranspiration of a Florida, U.S.A., freshwater wetland, *J. Hydrol.*, *74*(3–4), 355–371, doi:10.1016/0022-1694(84)90024-6.

Godsey, S. E., and J. Kirchner (2014), Dynamic, discontinuous stream networks: Hydrologically driven variations in active drainage density, flowing channels, and stream order, *Hydrol. Processes*, *28*(23), 5791–5803, doi:10.1002/hyp.10310.

Graham, C. B., H. R. Barnard, K. L. Kavanagh, and J. P. McNamara (2013), Catchment scale controls the temporal connection of transpiration and diel fluctuations in streamflow, *Hydrol. Processes*, *27*(18), 2541–2556, doi:10.1002/hyp.9334.

Gribovszki, Z., P. Kalicz, J. Szilágyi, and M. Kucsara (2008), Riparian zone evapotranspiration estimation from diurnal groundwater level fluctuations, *J. Hydrol.*, *349*(1–2), 6–17, doi:10.1016/j.jhydrol.2007.10.049.

Gribovszki, Z., J. Szilágyi, and P. Kalicz (2010), Diurnal fluctuations in shallow groundwater levels and streamflow rates and their interpretation—A review, *J. Hydrol.*, *385*(1–4), 371–383, doi:10.1016/j.jhydrol.2010.02.001.

Hays, K. B. (2003), Water use by saltcedar (Tamarix sp.) and associated vegetation on the Canadian, Colorado and Pecos rivers in Texas, PhD thesis, Texas A & M Univ., College Station.

Hock, R. (2005), Glacier melt: A review of processes and their modelling, *Prog. Phys. Geogr.*, *29*(3), 362–391, doi:10.1191/0309133305pp453ra.

Ingelrest, F., G. Barrenetxea, G. Schaefer, M. Vetterli, O. Couach, and M. B. Parlange (2010), SensorScope: Application-specific sensor network for environmental monitoring, *ACM Trans. Sensor Networks*, *6*(2), 1–32, doi:10.1145/1689239.1689247.

Jost, G., R. D. Moore, R. Smith, and D. R. Gluns (2012), Distributed temperature-index snowmelt modelling for forested catchments, *J. Hydrol.*, *420–421*, 87–101, doi:10.1016/j.jhydrol.2011.11.045.

Kane, D., R. Gieck, and L. Hinzman (1997), Snowmelt modeling at small Alaskan Arctic watershed, *J. Hydrol. Eng.*, *2*(4), 204–210, doi:10.1061/(ASCE)1084-0699(1997)2:4(204).

Katul, G. G., and M. B. Parlange (1992), Estimation of bare soil evaporation using skin temperature measurements, *J. Hydrol.*, *132*(1), 91–106, doi:10.1016/0022–1694(92)90174-T.

Kirchner, J. W. (2009), Catchments as simple dynamical systems: Catchment characterization, rainfall-runoff modeling, and doing hydrology backward, *Water Resour. Res.*, *45*, W02429, doi:10.1029/2008WR006912.

Kobayashi, D., and H. Motoyama (1984), Effect of snow cover on time lag of runoff from a watershed, *Ann. Glaciol.*, *6*, 123–125.

Kustas, W. P., A. Rango, and R. Uijlenhoet (1994), A simple energy budget algorithm for the snowmelt runoff model, *Water Resour. Res.*, *30*(5), 1515–1527, doi:10.1029/94WR00152.

Lehning, M., I. Vöksch, D. Gustafsson, T. A. Nguyen, M. Stähli, and M. Zappa (2006), ALPINE3D: A detailed model of mountain surface processes and its application to snow hydrology, *Hydrol. Processes*, *20*(10), 2111–2128, doi:10.1002/hyp.6204.

Loheide, S. P., II (2008), A method for estimating subdaily evapotranspiration of shallow groundwater using diurnal water table fluctuations, *Ecohydrology*, *1*(1), 59–66, doi:10.1002/eco.7.

Loheide, S. P., II, and S. M. Gorelick (2006), Quantifying stream–aquifer interactions through the analysis of remotely sensed thermographic profiles and in situ temperature histories, *Environ. Sci. Technol.*, *40*(10), 3336–3341, doi:10.1021/es0522074.

Loheide, S. P., II, and J. D. Lundquist (2009), Snowmelt-induced diel fluxes through the hyporheic zone, *Water Resour. Res.*, *45*, W07404, doi:10.1029/2008WR007329.

Lundquist, J. D., and D. R. Cayan (2002), Seasonal and spatial patterns in diurnal cycles in streamflow in the Western United States, *J. Hydrometeorol.*, *3*(5), 591–603, doi:10.1175/1525–7541(2002)003<0591:SASPID>2.0.CO;2.

Lundquist, J. D., and M. D. Dettinger (2005), How snowpack heterogeneity affects diurnal streamflow timing, *Water Resour. Res.*, *41*, W05007, doi:10.1029/2004WR003649.

Lundquist, J. D., M. D. Dettinger, and D. R. Cayan (2005), Snow-fed streamflow timing at different basin scales: Case study of the Tuolumne River above Hetch Hetchy, Yosemite, California, *Water Resour. Res.*, *41*, W07005, doi:10.1029/2004WR003933.

Martinec, J. (1989), Hour-to-hour snowmelt rates and lysimeter outflow during an entire ablation period, in *Snow Cover and Glacier Variations (Proceedings of the Baltimore Symposium)*, IAHS publication nr 183, edited by S. C. Colbeck, vol. 183, pp. 19–28, Baltimore, Md.
McGlynn, B. L., and J. Seibert (2003), Distributed assessment of contributing area and riparian buffering along stream networks, *Water Resour. Res.*, *39*(4), 1082, doi:10.1029/2002WR001521.
McLaughlin, D. L., and M. J. Cohen (2011), Thermal artifacts in measurements of fine-scale water level variation, *Water Resour. Res.*, *47*, W09601, doi:10.1029/2010WR010288.
Meyboom, P. (1965), Three observations on streamflow depletion by phreatophytes, *J. Hydrol.*, *2*(3), 248–261, doi:10.1016/0022–1694(65)90040-5.
Mutzner, R., E. Bertuzzo, P. Tarolli, S. V. Weijs, L. Nicotina, S. Ceola, N. Tomasic, I. Rodriguez-Iturbe, M. B. Parlange, and A. Rinaldo (2013), Geomorphic signatures on Brutsaert base flow recession analysis, *Water Resour. Res.*, *49*, 5462–5472, doi:10.1002/wrcr.20417.
Nadeau, D., W. Brutsaert, M. Parlange, E. Bou-Zeid, G. Barrenetxea, O. Couach, M. O. Boldi, J. Selker, and M. Vetterli (2009), Estimation of urban sensible heat flux using a dense wireless network of observations, *Environ. Fluid Mech.*, *9*(6), 635–653, doi:10.1007/s10652-009-9150-7.
O'Callaghan, J. F., and D. M. Mark (1984), The extraction of drainage networks from digital elevation data, *Comput. Vision Graphics Image Process.*, *28*(3), 323–344, doi:10.1016/s0734-189x(84)80011-0.
Orellana, F., P. Verma, S. P. Loheide, and E. Daly (2012), Monitoring and modeling water-vegetation interactions in groundwater-dependent ecosystems, *Rev. Geophys.*, *50*, RG3003, doi:10.1029/2011RG000383.
Parlange, M. B., and G. G. Katul (1992), Estimation of the diurnal variation of potential evaporation from a wet bare soil surface, *J. Hydrol.*, *132*(1–4), 71–89, doi:10.1016/0022-1694(92)90173-S.
Parlange, M. B., W. E. Eichinger, and J. D. Albertson (1995), Regional scale evaporation and the atmospheric boundary layer, *Rev. Geophys.*, *33*(1), 99–124, doi:10.1029/94RG03112.
Penna, D., H. J. Tromp-van Meerveld, A. Gobbi, M. Borga, and G. Dalla Fontana (2011), The influence of soil moisture on threshold runoff generation processes in an alpine headwater catchment, *Hydrol. Earth Syst. Sci.*, *15*(3), 689–702, doi:10.5194/hess-15-689-2011.
Pfister, L., J. J. McDonnell, C. Hissler, and L. Hoffmann (2010), Ground-based thermal imagery as a simple, practical tool for mapping saturated area connectivity and dynamics, *Hydrol. Processes*, *24*(21), 3123–3132, doi:10.1002/hyp.7840.
Reusser, D. E., T. Blume, B. Schaefli, and E. Zehe (2009), Analysing the temporal dynamics of model performance for hydrological models, *Hydrol. Earth Syst. Sci.*, *13*(7), 999–1018, doi:10.5194/hess-13-999-2009.
Rigon, R., G. Bertoldi, and T. M. Over (2006), GEOtop: A distributed hydrological model with coupled water and energy budgets, *J. Hydrometeorol.*, *7*(3), 371–388.
Ronan, A. D., D. E. Prudic, C. E. Thodal, and J. Constantz (1998), Field study and simulation of diurnal temperature effects on infiltration and variably saturated flow beneath an ephemeral stream, *Water Resour. Res.*, *34*(9), 2137–2153, doi:10.1029/98WR01572.
Simoni, S., S. Padoan, D. F. Nadeau, M. Diebold, A. Porporato, G. Barrenetxea, F. Ingelrest, M. Vetterli, and M. B. Parlange (2011), Hydrologic response of an alpine watershed: Application of a meteorological wireless sensor network to understand streamflow generation, *Water Resour. Res.*, *47*, W10524, doi:10.1029/2011WR010730.
Singh, P., U. K. Haritashya, K. S. Ramasastri, and N. Kumar (2005), Diurnal variations in discharge and suspended sediment concentration, including runoff-delaying characteristics, of the Gangotri Glacier in the Garhwal Himalayas, *Hydrol. Processes*, *19*(7), 1445–1457, doi:10.1002/hyp.5583.
Soylu, M. E., J. D. Lenters, E. Istanbulluoglu, and S. P. Loheide (2012), On evapotranspiration and shallow groundwater fluctuations: A Fourier-based improvement to the White method, *Water Resour. Res.*, *48*, W06506, doi:10.1029/2011WR010964.
Stagnitti, F., J.-Y. Parlange, and C. W. Rose (1989), Hydrology of a small wet catchment, *Hydrol. Processes*, *3*(2), 137–150, doi:10.1002/hyp.3360030204.
Szilágyi, J., Z. Gribovszki, P. Kalicz, and M. Kucsara (2008), On diurnal riparian zone groundwater-level and streamflow fluctuations, *J. Hydrol.*, *349*(1–2), 1–5, doi:10.1016/j.jhydrol.2007.09.014.
Tarolli, P. (2014), High-resolution topography for understanding Earth surface processes: Opportunities and challenges, *Geomorphology*, *216*, 295–312, doi:10.1016/j.geomorph.2014.03.008.
Thibaud, E., R. Mutzner, and A. C. Davison (2013), Threshold modeling of extreme spatial rainfall, *Water Resour. Res.*, *49*, 4633–4644, doi:10.1002/wrcr.20329.
Tobin, C., B. Schaefli, L. Nicotina, S. Simoni, G. Barrenetxea, R. Smith, M. Parlange, and A. Rinaldo (2013), Improving the degree-day method for sub-daily melt simulations with physically-based diurnal variations, *Adv. Water Resour.*, *55*, 149–164, doi:10.1016/j.advwatres.2012.08.008.
Tsang, Y.-P., G. Hornberger, L. A. Kaplan, J. D. Newbold, and A. K. Aufdenkampe (2014), A variable source area for groundwater evapotranspiration: Impacts on modeling stream flow, *Hydrol. Processes*, *28*(4), 2439–2450, doi:10.1002/hyp.9811.
Tschinkel, H. M. (1963), Short-term fluctuation in streamflow as related to evaporation and transpiration, *J. Geophys. Res.*, *68*(24), 6459–6469, doi:10.1029/JZ068i024p06459.
Webb, E. K., G. I. Pearman, and R. Leuning (1980), Correction of flux measurements for density effects due to heat and water vapour transfer, *Q. J. R. Meteorol. Soc.*, *106*(447), 85–100, doi:10.1002/qj.49710644707.
Weijs, S. V., R. Mutzner, and M. B. Parlange (2013), Could electrical conductivity replace water level in rating curves for alpine streams?, *Water Resour. Res.*, *49*, 343–351, doi:10.1029/2012WR012181.
Weisman, R. N. (1977), The effect on evapotranspiration on streamflow recession, *Hydrol. Sci. Bull.*, *22*(3), 371–377, doi:10.1080/02626667709491731.
White, W. N. (1932), Method of estimating ground-water supplies based on discharge by plants and evaporation from soil —Results of investigation in Escalante Valley, Utah, *U.S. Geol. Surv. Water Supply Pap.*, *659-A*, 1–105.
Wondzell, S. M., M. N. Gooseff, and B. L. McGlynn (2007), Flow velocity and the hydrologic behavior of streams during baseflow, *Geophys. Res. Lett.*, *34*, L24404, doi:10.1029/2007GL031256.